Hole transporting material-free and annealing-free thermal evaporated planar perovskite solar cells with an ultra-thin $CH_3NH_3PbI_{3−X}Cl_X$ layer

Zisheng Su [a,*], Fuhua Hou [a,b], Fangming Jin [a,b], Lidan Wang [c], Yantao Li [a], Jianzhuo Zhu [d], Bei Chu [a,*], Wenlian Li [a]

[a] State Key Laboratory of Luminescence and Applications, Changchun Institute of Optics, Fine Mechanics and Physics, Chinese Academy of Sciences, Changchun 130033, PR China
[b] University of Chinese Academy of Sciences, Beijing 100039, PR China
[c] State Key Laboratory of Electroanalytic Chemistry, Changchun Institute of Applied Chemistry, Chinese Academy of Sciences, Changchun 130022, PR China
[d] College of Science, Yanshan University, Qinhuangdao 066004, PR China

ARTICLE INFO

ABSTRACT

High efficiency and stable hole transporting material-free (HTM-free) planar heterojunction (PHJ) perovskite solar cells are constructed by directly thermal evaporating perovskite materials onto indium tin oxide substrate. A condense and homogeneous morphology is found for this perovskite film even without any annealing process. The optimized HTM-free $CH_3NH_3PbI_{3−X}Cl_X/C_{60}$ PHJ device with a 35 nm ultra-thin $CH_3NH_3PbI_{3−X}Cl_X$ layer presents a high hole extraction efficiency and a low charge carrier recombination probability, which results in a high short circuit current and fill factor. The HTM-free device shows a high power conversion efficiency of 8.37%, which is one of the highest efficiency among reported inverted HTM-free perovskite solar cells even that a thinner perovskite film is used. More importantly, the device also exhibits a superior stability in ambient conditions.

© 2015 Elsevier B.V. All rights reserved.

1. Introduction

Organometal halide perovskites ($CH_3NH_3PbI_3$ and $CH_3NH_3PbI_{3−X}Cl_X$) have recently attracted tremendous attention as promising materials for hybrid solar cells owing to their direct bandgap, high absorption coefficient, long exciton diffusion length, and excellent charge transport property [1–7]. By utilizing these superior properties, high performance perovskite solar cells with power conversion efficiency (PCE) higher than 15% have been realized. There are two typical device structures for organometal halide based perovskite solar cells, meso-structured and planar heterojunction (PHJ) solar cells. For meso-superstructured solar cells, the perovskite materials are infiltrated into a metal oxide scaffold layer. The inhomogeneous infiltration of perovskite materials leads to a low PCE and reproducibility in such a configuration [8]. Besides, the preparation of the meal oxide scaffold layers usually requires a high temperature sintering process, which limits their applications in flexible substrates. The PHJ solar cells with the perovskite sandwiched between hole- and electron-conductors avoid the pore-filling problem and high temperature process without sacrificing efficiency compared to the meso-superstructured ones. Poly(3,4-ethylene dioxythiophene):poly(styrene sulfonate) (PEDOT:PSS) is usually used as the hole transporting materials (HTM) in the PHJ perovskite solar cells and high PCEs were obtained [9–12]. However, the acidic PEDOT:PSS can etch ITO and decompose perovskite, which results in poor stability of the devices [13]. Some other robust materials, such as polymers [14,15], inorganic materials [16–18], and bilayer complex structures [19,20], have been adopted as the alternatives to PEDOT:PSS. However, their PCEs are still lower than that of state of the art ones based on PEDOT:PSS. While most research attention has been drawn into pursuing higher PCE of these perovskite solar cells, the material cost should also be considered as an important factor governing the practical application of this promising technology. Recently, HTM-free perovskite solar cells have drawn more and more attention benefited for their simpler device structure and lower cost, and PCEs in the range of 5–12% are obtained [21–24]. However, there has rare HTM-free inverted perovskite solar cells with perovskite materials deposited directly on transparent conductor oxides (TCO), such as indium tin oxide (ITO) and fluorine doped tin oxide. Tsai et al. [25] fabricated an inverted HTM-free PHJ perovskite solar cell with a PCE of 11.02% by a solution process. Hu et al. [26] demonstrated an inverted HTM-free PHJ perovskite solar cell with a simple thermal evaporated perovskite/C_{60} bilayer structure, which presented a PCE of 5.4%. Ng et al. [27] reported

* Corresponding authors.
E-mail addresses: suzs@ciomp.ac.cn (Z. Su), chub@ciomp.ac.cn (B. Chu).

that the PCE can be increased to 6.1% via adopting 4,7-diphenyl-1,10-phenanthroline (Bphen) as the hole blocking layer. However, their PCEs are still lower and should be further improved.

The PCE of a perovskite solar cell strongly correlates to the coverage, thickness, quality, and transport properties of the perovskite film. Perovskite films can be prepared by solution process via one-step or two-step solution depositions [2,3] and vacuum thermal evaporation [4,26–28]. Among these methods, the vacuum thermal evaporation forms a perovskite film with the most homogeneous morphology and the highest coverage, leading to a higher PCE of the corresponding devices. In these devices, a thick perovskite film of about 300 nm was usually used. Such a thick layer consumes a large amount of materials and a long process time, which indicates that the solar cells with a thin perovskite layer are more economical from the cost point of view. Besides, all these reported thermal evaporated perovskite layers included a thermal annealing process, which makes the fabrication process more complex. Recently, semitransparent solar cells with a thin or island-like perovskite layer have drawn more and more attention because of their potential applications in building-integrated photovoltaics [29–32]. However, their PCEs are still lower and should be further improved, which firstly demands that the solar cell with a thin perovskite layer presents a high PCE.

In this work, HTM-free and annealing-free inverted PHJ perovskite solar cells are constructed by directly thermal co-evaporating CH_3NH_3I and $PbCl_2$ onto ITO substrate. The $CH_3NH_3PbI_{3-x}Cl_X/C_{60}$ PHJ device with a 35 nm ultra-thin $CH_3NH_3PbI_{3-x}Cl_X$ layer exhibits a high short circuit current (J_{SC}) and fill factor (FF), indicating a high hole extraction efficiency and low charge carrier recombination probability of the device. Consequently, a high PCE of 8.37% is demonstrated. To the best of our knowledge, this is one of the highest PCE for the perovskite solar cells with the perovskite layer directly deposited on a TCO.

2. Experimental details

Devices were fabricated on patterned ITO coated glass substrates with a sheet resistance of 15 Ω/sq. The substrates were routinely cleaned followed by UV-ozone treatment for 10 min. The structure of the HTM-free PHJ perovskite solar cells is shown in Fig. 1(a). The optimized device has a structure of ITO/$CH_3NH_3PbI_{3-x}Cl_X$/C_{60} (40 nm)/Bphen (5 nm)/Al (100 nm), and the thickness of $CH_3NH_3PbI_{3-x}Cl_X$ was varied from 26 to 52 nm. All layers were sequentially deposited onto the substrates by thermal evaporation in a vacuum chamber at a pressure of 5×10^{-4} Pa without breaking vacuum. The $CH_3NH_3PbI_{3-x}Cl_X$ film was grown by thermal co-evaporating CH_3NH_3I and $PbCl_2$. The molar ratio of

$CH_3NH_3I/PbCl_2$ was varied and optimized to be 6:1 in our experiment. For this co-evaporation process, $PbCl_2$ was first heated. After a steady deposition rate of 0.01 Å/s was reached, CH_3NH_3I was then heated until a steady deposition rate of 0.25 Å/s was obtained. Then the shuttle mask was opened to ensure that the two precursors were evaporated simultaneously. Deposition rates were kept at 1 Å/s for C_{60} and Bphen and 5 Å/s for Al cathode. Deposition rate and layer thickness were monitored in situ using oscillating quartz monitors.

X-ray diffraction (XRD) patterns were measured with a Rigaku D/Max-2500 diffractometer using Cu Kα radiation (λ = 1.54 Å). Absorption spectra were recorded on a Shimadzu 3101 spectrophotometer. Scanning electron microscopy (SEM) images were measured by a Hitachi S4800 field emission scanning electron microscopy. The surface topographies were imaged with a Bruker MultiMode 8 atomic force microscope (AFM) in tapping mode. Film thicknesses were measured by an Avantes XP-1 surface profiler. Current–voltage (J–V) characteristics of the devices were measured with a Keithley 2400 source meter both in dark and under illumination of a Xe lamp light source with an AM 1.5G filter, and the irradiation intensity was certified to be of 100 mW/cm^2. The voltage scans were swept from short circuit to forward bias with a rate of 0.05 V/s. The incident photon to current conversion efficiency (IPCE) spectra were performed with a Stanford SR803 lock-in amplifier under monochromatic illumination. All measurements were performed under ambient conditions.

3. Results and discussions

Fig. 2(a) shows the XRD pattern of $CH_3NH_3PbI_{3-x}Cl_X$ film (35 nm) on an ITO substrate. Diffraction peaks of 2θ at about 14.05°, 28.26°, and 42.95° are found, which can be assigned to the (1 1 0), (2 2 0), and (3 3 0) planes of $CH_3NH_3PbI_3$, respectively [5]. Moreover, no diffraction peaks of PbI_2, $PbCl_2$, and $CH_3NH_3PbCl_3$ is found, indicating good conversion from the precursors to perovskite and high purity of this perovskite film. Fig. 2(b) depicts the absorption spectra of the $CH_3NH_3PbI_{3-x}Cl_X$ (35 nm), C_{60} (40 nm), and $CH_3NH_3PbI_{3-x}Cl_X$ (35 nm)/C_{60} (40 nm) films. Both $CH_3NH_3PbI_{3-x}Cl_X$ and C_{60} appears an absorption band in visible region, and an absorption onset of about 780 nm is found for $CH_3NH_3PbI_{3-x}Cl_X$, which corresponds to a bandgap of 1.59 eV.

Compared with solution-processed perovskite solar cells, the devices fabricated with a vacuum thermal evaporation method show a higher coverage, which avoids direct contact between hole-conductor and electron-conductor. Such a characteristic is more critical for HTM-free devices, as the direct contact between anode and electron-conductor will result in electron transporting to anode and hence an increased hole–electron recombination
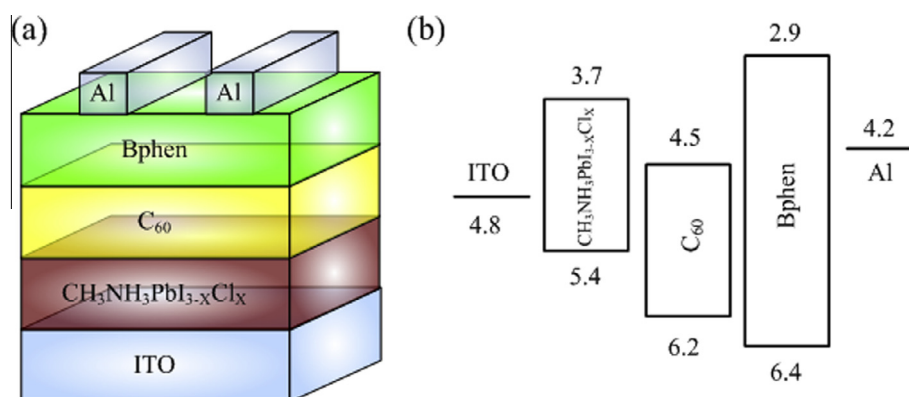

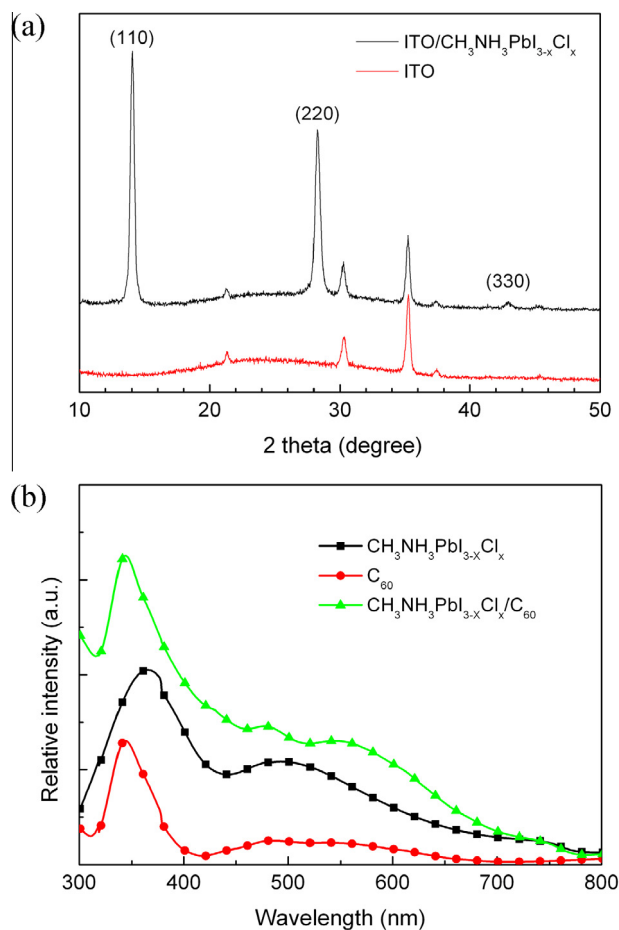**Fig. 1.** (a) Structure and (b) schematic energy level diagram of the device.

Fig. 2. (a) XRD patterns of ITO/CH$_3$NH$_3$PbI$_{3-X}$Cl$_X$ and ITO substrate. (b) Absorption spectra of CH$_3$NH$_3$PbI$_{3-X}$Cl$_X$, C$_{60}$, and CH$_3$NH$_3$PbI$_{3-X}$Cl$_X$/C$_{60}$ films on ITO substrates.

Fig. 4. (a) J–V curves and (b) IPCE spectra of the devices with different thickness of CH$_3$NH$_3$PbI$_{3-X}$Cl$_X$.

probability. Fig. 3(a) displays the SEM image of the CH$_3$NH$_3$PbI$_{3-X}$Cl$_X$ film (35 nm) formed by directly thermal evaporated onto an ITO substrate. A condense and homogeneous morphology is found for this film. The root mean square (RMS) roughness is 6.14 nm, as shown in the AFM image in Fig. 3(b). Such a RMS roughness is lower than the counterpart ones prepared by a solution process, which is favorable for constructing PHJ solar cells.

The J–V curves of the perovskite solar cells with different thickness of CH$_3$NH$_3$PbI$_{3-X}$Cl$_X$ are presented in Fig. 4(a). Each curve is averaged from 3 to 12 cells of 1–4 batches. Table 1 lists the parameters of these devices extracted from their J–V curves. The devices exhibit a comparable open-circuit voltage (V_{OC})
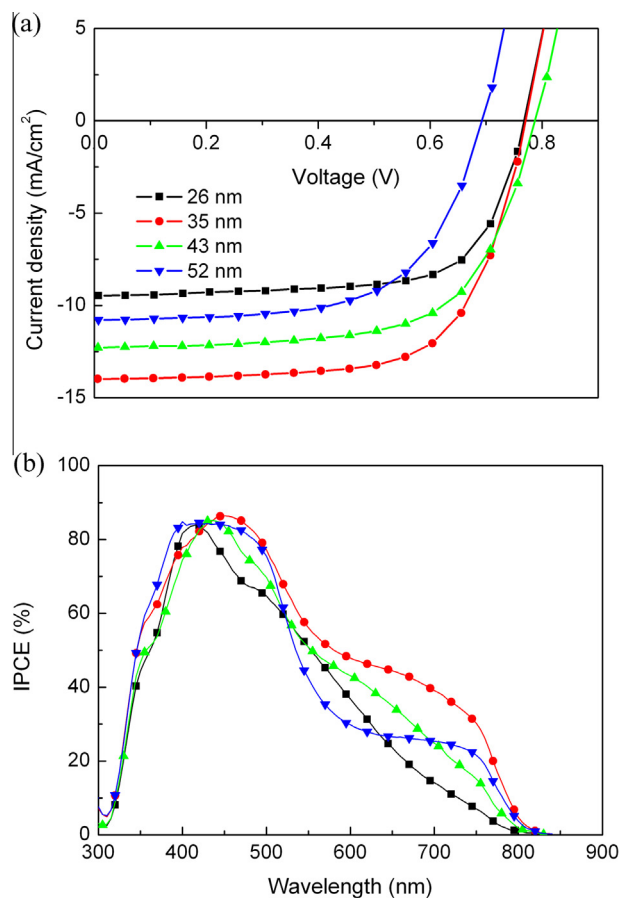
except the one with a thick CH$_3$NH$_3$PbI$_{3-X}$Cl$_X$ layer of 52 nm. However, the J_{SC} of the devices increases with increasing thickness of CH$_3$NH$_3$PbI$_{3-X}$Cl$_X$ from 26 to 35 nm, and further increase of the thickness leads to a slightly decrease of J_{SC}. On contrast, the FF shows a monotone decrease with increasing thickness of CH$_3$NH$_3$PbI$_{3-X}$Cl$_X$, which suggests an increased charge carrier recombination in the devices. The increase of the charge carrier recombination would also cause the decrease of J_{SC} and V_{OC} of the devices with a thick CH$_3$NH$_3$PbI$_{3-X}$Cl$_X$ layer. It has been reported that electron and hole diffusion lengths of chloride-based perovskite films are over 1 μm [33]. This suggests that the electron and hole diffusion lengths of our perovskite films are smaller, which may be attributed to the small grain size of the perovskite films, as shown in Fig. 3(a). The optimized
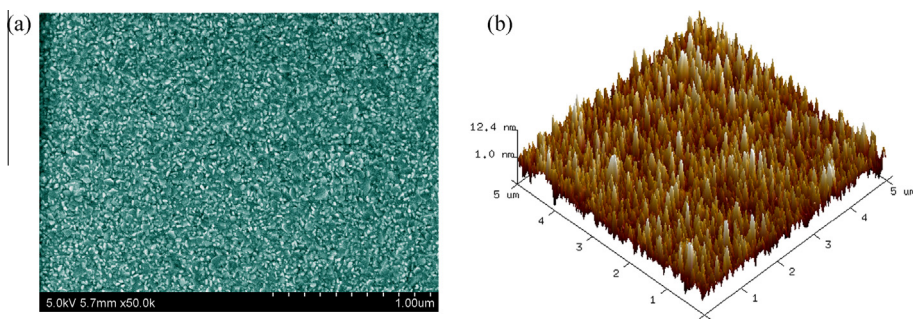

Fig. 3. (a) SEM and (b) AFM images of a CH$_3$NH$_3$PbI$_{3-X}$Cl$_X$ layer on an ITO substrate.

Table 1
Photovoltaic parameters of the devices with different thickness of $CH_3NH_3PbI_{3-X}Cl_X$.

Thickness (nm)	J_{SC} (mA/cm^2)	V_{OC} (V)	FF	PCE (%)	Number of cells (batches)
26	9.46 ± 0.35	0.77 ± 0.01	0.69 ± 0.03	5.03 ± 0.31	6 (2)
35	13.98 ± 0.90	0.77 ± 0.02	0.68 ± 0.03	7.27 ± 0.73	12 (4)
43	12.27 ± 0.73	0.79 ± 0.01	0.65 ± 0.04	6.29 ± 0.40	6 (2)
52	10.79 ± 1.24	0.69 ± 0.01	0.63 ± 0.02	4.65 ± 0.65	3 (1)

device with a 35 nm $CH_3NH_3PbI_{3-X}Cl_X$ shows a J_{SC}, V_{OC}, and FF of 13.98 mA/cm^2, 0.77 V, and 0.68, respectively, corresponding to a PCE of 7.27%. The high J_{SC} and FF indicate that the device has a high hole extraction efficiency at the ITO/$CH_3NH_3PbI_{3-X}Cl_X$ interface and a low charge carrier recombination probability in the device. It should be noted that the V_{OC} of these HTM-free devices is lower than the ones with a PEDOT:PSS HTM [9–12]. Fig. 1(b) displays the schematic energy level diagram of the device, and energy level data was cited from ref [34–36]. The valence band maximum (VBM) of $CH_3NH_3PbI_{3-X}Cl_X$ is 5.4 eV, while the work-function of ITO electrode is 4.8 eV. There is a 0.6 eV energy offset between the work-function of ITO and VBM of $CH_3NH_3PbI_{3-X}Cl_X$. Such an energy offset may constrain the built-in field and thus result in the thermionic losses for holes and hence a loss in V_{OC} [36,37]. This suggests that a higher PCE can be expected for these HTM-free perovskite solar cells if a TCO electrode with a higher work-function were used. Fig. 4(b) shows the IPCE spectra of the devices. A maximum value of about 90% is obtained at 440 nm in the device with a 35 nm $CH_3NH_3PbI_{3-X}Cl_X$. The calculated J_{SC} from IPCE spectra of the devices with 26, 35, 43, and 52 nm perovskite layers are 10.17, 14.01, 11.76, and 11.40 mA/cm^2, respectively. All these value are within the error compared with that from their respective J–V curves. Due to the no-excitonic nature of perovskite materials, free charge carriers can be formed directly in the bulk of $CH_3NH_3PbI_{3-X}Cl_X$ upon illumination [14]. On the other hands, in term of the energy level diagram shown in Fig. 1(b), the energy level offsets between VBM of $CH_3NH_3PbI_{3-X}Cl_X$ and the highest occupied molecular orbit of C_{60} is 0.8 eV. This energy level offset ensure that the excitons of C_{60} can be dissociated in the $CH_3NH_3PbI_{3-X}Cl_X/C_{60}$ interface. Thus both $CH_3NH_3PbI_{3-X}Cl_X$ and C_{60} contribute to the high photocurrent of the devices as both of them absorb in the visible region, which is evidenced by the absorption spectra shown in Fig. 2(b).
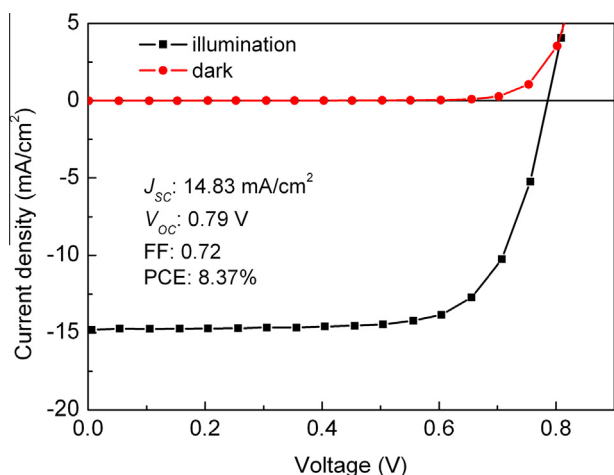
Fig. 5 shows the J–V curves of the best device with a 35 nm $CH_3NH_3PbI_{3-X}Cl_X$ under illumination and in dark. The device shows a J_{SC}, V_{OC}, FF, and PCE of 14.83 mA/cm^2, 0.79 V, 0.72, and 8.37%, respectively. To the best of our knowledge, this is the highest PCE for thermal-evaporated HTM-free perovskite solar cells with a perovskite layer deposited directly on TCOs [26,27]. Moreover, such a PCE is comparable and even a slight higher than some other recently reported HTM-free perovskite solar cells despite that an ultra-thin $CH_3NH_3PbI_{3-X}Cl_X$ layer is used here [21–24]. It has been reported that the post-thermal annealing process will increase of the grain size of the perovskite material and hence the exciton diffusion length and charge carriers mobilities [4]. Thus a higher PCE can be expected if a post-thermal annealing process were adopted for our devices.

We have also tried to fabricate solar cells through a two-step solution process. Although a PCE of about 10% was obtained when PEDOT:PSS was used as the HTM [19], the HTM-free device prepared with the some processes presented a poor performance. This should be attributed to its lower coverage of the perovskite film when it was deposited directly onto ITO substrate by a solution method. Similar low performance was reported by other groups with the same strategy [17]. This suggests that the coverage of the perovskite film plays an important role in determining the performance of a HTM-free inverted perovskite solar cell. Because it is easy to form a perovskite film with a high coverage and smooth morphology, the vacuum thermal evaporation method is more favorable for constructing HTM-free PHJ perovskite solar cells.

Stability is another important factor that limited the practical application of perovskite solar cells. Fresh solar cell with a 35 nm $CH_3NH_3PbI_{3-X}Cl_X$ was aged under illumination of natural light in ambient condition (humidity of about 30% and temperature of 25 °C) without encapsulation. The J–V curves of the device under AM 1.5G 100 mW/cm^2 irradiation with different aging times are shown in Fig. 6(a). Device performance parameters extracted from the J–V curves are illuminated in Fig. 6(b). All the parameters decrease with the aging time except V_{OC}, which shows a slightly increase. The PCE decreases to half of its initial value after about 150 h, which is primary attributed to the degradation of J_{SC}. It was reported that the perovskite layers are very sensitive to moisture, which may react with perovskite and result in the decomposition of perovskite [38,39]. This indicates that the HTM has a dramatic impact on the stability of perovskite solar cells [40]. As we are failure to obtained perovskite solar cells by vacuum thermal evaporating perovskite layer onto PEDOT:PSS HTM layer and there was no report about such a device, it is difficult to compare the stability between the HTM-free device and the one with a PEDOT:PSS layer. However, the PCE of the device prepared by solution process with a PEDOT:PSS HTM decreased to half of its initial value within 50 h and completely failure within 120 h [13]. The water-soluble nature will lead to the absorption of moisture in the PEDOT:PSS layer, which may accelerate the decomposition of perovskite. Besides, the acidic PEDOT:PSS may also etch ITO and result in diffusion of In ions into the photoactive layer [41]. Compared with this device, our HTM-free perovskite solar cells exhibit a more promising stability.
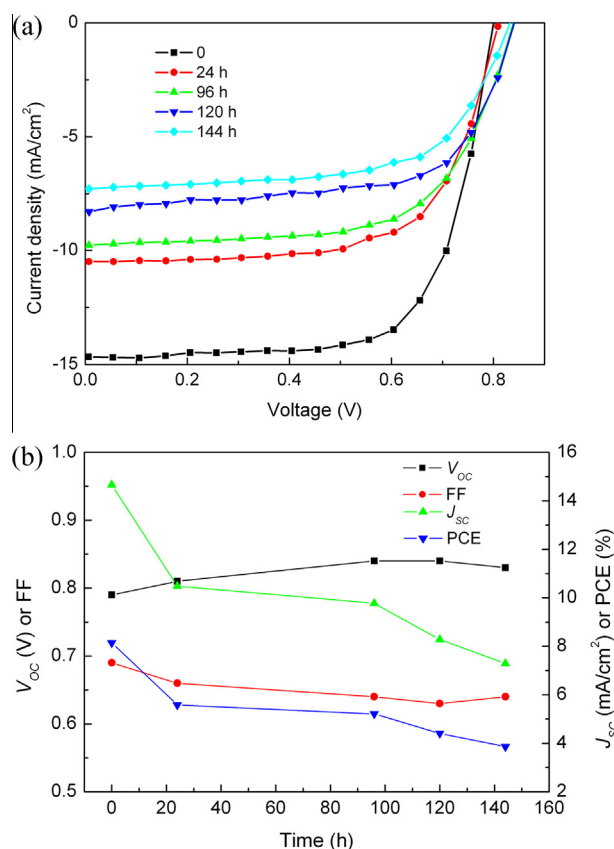

Fig. 5. J–V curves of the best device with a 35 nm $CH_3NH_3PbI_{3-X}Cl_X$ under illumination and in dark.

Fig. 6. (a) J–V curves of the device with different aging times. (b) Photovoltaic parameters as a function of aging time for the device with a 35 nm $CH_3NH_3PbI_{3-X}Cl_X$.

4. Conclusion

In summary, HTM-free and annealing-free inverted PHJ perovskite solar cells were firstly fabricated by directly thermal co-evaporating CH_3NH_3I and $PbCl_2$ onto ITO substrates. A condense and homogeneous morphology is found for this $CH_3NH_3PbI_{3-X}Cl_X$ film. The $CH_3NH_3PbI_{3-X}Cl_X/C_{60}$ PHJ device with a 35 nm ultra-thin $CH_3NH_3PbI_{3-X}Cl_X$ layer exhibits a champion PCE up to 8.37%. To the best of our knowledge, this is the highest PCE for the HTM-free perovskite solar cells with a perovskite layer thermal deposited directly on TCOs. A higher PCE can be expected for the devices with a well controlled morphology through optimizing deposition conditions (such as deposition rate, contents of precursors, and post-thermal annealing) of the perovskites to increase their charge carrier mobilities and exciton diffusion lengths and a high work-function TCO electrode to minimize thermionic losses for holes. Moreover, the HTM-free perovskite solar cells exhibit a superior stability compared with the one with a PEDOT:PSS HTM. This work provides a new strategy to construct simple but efficient and stable perovskite solar cells. Besides, such a structure can also be adopted to fabricate semitransparent perovskite solar cells if a transparent cathode were used.

Acknowledgements

References

[1] A. Kojima, K. Teshima, Y. Shirai, T. Miyasaka, J. Am. Chem. Soc. 131 (2009) 6050–6051.
[2] H.S. Kim, C.R. Lee, J.H. Im, K.B. Lee, T. Moehl, A. Marchioro, S.J. Moon, R. Humphry-Baker, J.H. Yum, J.E. Moser, M. Grätzel, N.G. Park, Sci. Rep. 2 (2012) 591.
[3] J. Burschka, N. Pellet, S.J. Moon, R. Humphry-Baker, P. Gao, M.K. Nazeeruddin, M. Grätzel, Nature 499 (2013) 316–319.
[4] M. Liu, M.B. Johnston, H.J. Snaith, Nature 501 (2013) 395–398.
[5] H. Zhou, Q. Chen, G. Li, S. Luo, T.B. Song, H.S. Duan, Z. Hong, J. You, Y. Liu, Y. Yang, Science 345 (2014) 542–546.
[6] N.J. Jeon, J.H. Noh, W.S. Yang, Y.C. Kim, S. Ryu, J. Seo, S.I. Seok, Nature 517 (2015) 476–480.
[7] W. Nie, H. Tsai, R. Asadpour, J.C. Blancon, A.J. Neukirch, G. Gupta, J.J. Crochet, M. Chhowalla, S. Tretiak, M.A. Alam, H.L. Wang, A.D. Mohite, Science 247 (2015) 522–525.
[8] G.E. Eperon, V.M. Burlakov, P. Docampo, A. Goriely, H.J. Snaith, Adv. Funct. Mater. 24 (2014) 151–157.
[9] J.Y. Jeng, Y.F. Chiang, M.H. Lee, S.R. Peng, T.F. Guo, P. Chen, T.C. Wen, Adv. Mater. 25 (2013) 3727–3732.
[10] Z. Xiao, Q. Dong, C. Bi, Y. Shao, Y. Yuan, J. Huang, Adv. Mater. 26 (2014) 6503–6509.
[11] J. You, Y. Yang, Z. Hong, T.B. Song, L. Meng, Y. Liu, C. Jiang, H. Zhou, W.H. Chang, G. Li, Y. Yang, Appl. Phys. Lett. 105 (2014) 183902.
[12] L.Q. Zhang, X.W. Zhang, Z.G. Yin, Q. Jiang, X. Liu, J.H. Meng, Y.J. Zhao, H.L. Wang, J. Mater. Chem. A 3 (2015) 12133–12138.
[13] J.S. Yeo, R. Kang, S. Lee, Y.J. Jeon, N. Myoung, C.L. Lee, D.Y. Kim, J.M. Yun, Y.H. Seo, S.S. Kim, S.I. Na, Nano Energy 12 (2015) 96–104.
[14] Q. Lin, A. Armin, R.C.R. Nagiri, P.L. Burn, P. Meredith, Nat. Photonics 9 (2015) 106–112.
[15] D. Zhao, M. Sexton, H.Y. Park, G. Baure, J.C. Nino, F. So, Adv. Energy Mater. 4 (2014) 1401855.
[16] J.Y. Jeng, K.C. Chen, T.Y. Chiang, P.Y. Lin, T.D. Tsai, Y.C. Chang, T.F. Guo, P. Chen, T.C. Wen, Y.J. Hsu, Adv. Mater. 26 (2014) 4107–4113.
[17] Z. Wu, S. Bai, J. Xiang, Z. Yuan, Y. Yang, W. Cui, X. Gao, Z. Liu, Y. Jin, B. Sun, Nanoscale 6 (2014) 10505–10510.
[18] L. Hu, W. Wang, H. Liu, J. Peng, H. Cao, G. Shao, Z. Xie, W. Ma, J. Tang, J. Mater. Chem. A 3 (2015) 515–518.
[19] F. Hou, Z. Su, F. Jin, X. Yan, L. Wang, H. Zhao, J. Zhu, B. Chu, W. Li, Nanoscale 7 (2015) 9427–9432.
[20] B.S. Kim, T.M. Kim, M.S. Choi, H.S. Shim, J.J. Kim, Org. Electron. 17 (2015) 103–106.
[21] L. Etgar, P. Gao, Z. Xue, Q. Peng, A.K. Chandiran, B. Liu, M.K. Nazeeruddin, M. Grätzel, J. Am. Chem. Soc. 134 (2012) 17396–17399.
[22] J. Shi, J. Dong, S. Lv, Y. Xu, L. Zhu, J. Xiao, X. Xu, H. Wu, D. Li, Y. Luo, Q. Meng, Appl. Phys. Lett. 104 (2014) 063901.
[23] F. Hao, C.C. Stoumpos, Z. Liu, R.P.H. Chang, M.G. Kanatzidis, J. Am. Chem. Soc. 136 (2014) 16411–16419.
[24] A. Mei, X. Li, L. Liu, Z. Ku, T. Liu, Y. Rong, M. Xu, M. Hu, J. Chen, M. Grätzel, H. Han, Science 345 (2014) 295–298.
[25] K.W. Tsai, C.C. Chueh, S.T. Williams, T.C. Wen, A.K.Y. Jen, J. Mater. Chem. A 3 (2015) 9128–9132.
[26] H. Hu, D. Wang, Y. Zhou, J. Zhang, S. Lv, S. Pang, X. Chen, Z. Liu, N.P. Padture, G. Cui, RSC Adv. 4 (2014) 28964–28967.
[27] T.W. Ng, C.Y. Chan, M.F. Lo, Z.Q. Guan, C.S. Lee, J. Mater. Chem. A 3 (2015) 9081–9085.
[28] C.W. Chen, H.W. Kang, S.Y. Hsiao, P.F. Yang, K.M. Chiang, H.W. Lin, Adv. Mater. 26 (2014) 6647–6652.
[29] G.E. Eperon, V.M. Burlakov, A. Goriely, H.J. Snaith, ACS Nano 8 (2014) 591–598.
[30] C. Roldán-Carmona, O. Malinkiewicz, R. Betancur, G. Longo, C. Momblona, F. Jaramillo, L. Camacho, H.J. Bolink, Energy Environ. Sci. 7 (2014) 2968–2973.
[31] E.D. Gaspera, Y. Peng, Q. Hou, L. Spiccia, U. Bach, J.J. Jasieniak, Y.B. Cheng, Nano Energy 13 (2015) 249–257.
[32] F. Guo, H. Azimi, Y. Hou, T. Przybilla, M. Hu, C. Bronnbauer, S. Langner, E. Spiecker, K. Forberich, C.J. Brabec, Nanoscale 7 (2015) 1642–1649.
[33] S.D. Stranks, G.E. Eperon, G. Grancini, C. Menelaou, M.J.P. Alcocer, T. Leijtens, L.M. Herz, A. Petrozza, H.J. Snaith, Science 342 (2013) 341–344.
[34] P. Peumans, S.R. Forrest, Appl. Phys. Lett. 79 (2001) 126–128.
[35] S. Naka, H. Okada, H. Onnagawa, T. Tsutsui, Appl. Phys. Lett. 76 (2000) 197–199.
[36] P. Schulz, E. Edri, S. Kirmayer, G. Hodes, D. Cahen, A. Kahn, Energy Environ. Sci. 7 (2014) 1377–1381.
[37] Q.K. Wang, R.B. Wang, P.F. Shen, C. Li, Y.Q. Li, L.J. Liu, S. Duhm, J.X. Tang, Adv. Mater. Interfaces 2 (2015) 1400528.
[38] G. Niu, W. Li, F. Meng, L. Wang, H. Dong, Y. Qiu, J. Mater. Chem. A 2 (2014) 705–710.
[39] Y. Han, S. Meyer, Y. Dkhissi, K. Weber, J.M. Pringle, U. Bach, L. Spiccia, Y.B. Cheng, J. Mater. Chem. A 3 (2015) 8139–8147.
[40] J. Yang, B.D. Siempelkamp, D. Liu, T.L. Kelly, ACS Nano 9 (2015) 1955–1963.
[41] M.P. de Jong, L.J. van IJzendoorn, M.J.A. de Voigt, Appl. Phys. Lett. 77 (2000) 2255–2257.